water

Article

Model Test and Numerical Simulation of Slope Instability Process Induced by Rainfall

Yongshuai Sun [1,*], Ke Yang [2], Ruilin Hu [3], Guihe Wang [4] and Jianguo Lv [4]

1 College of Water Resources & Civil Engineering, China Agricultural University, Beijing 100083, China
2 Land and Resources Exploration Center, Hebei Bureau of Geology and Mineral Resources Exploration, Shijiazhuang 050081, China
3 Key Laboratory of Shale Gas and Geoengineering, Institute of Geology and Geophysics, Chinese Academy of Sciences, Beijing 100029, China
4 School of Engineering and Technology, China University of Geosciences, Beijing 100083, China
* Correspondence: causys666@163.com

Abstract: Due to rainfall infiltration, slope instability becomes frequent, which is the main reason for landslide disasters. In this study, the stability of slope affected by rainfall was analyzed using an indoor model test and geo-studio simulation method, and the variation law of phreatic line, seepage field, the most dangerous sliding surface, and safety factor with time were studied under rainfall infiltration. Research results showed that under the effect of rainfall, the slope failure presented a typical traction development mode. With the increase of time, the phreatic line of the slope kept rising, the water head keeps increasing, the seepage depth in the slope became deeper, and the slope stability worsened until the slope was damaged. The water head height decreased gradually from the slope left boundary to the right, and the water head width decreased gradually. The soil at the slope back edge was damaged, and the sliding soil accumulated at the slope foot, forming a gentle slope, which increased the shear strength of the slope, making the slope finally reach a stable state. In this process, the overlying soil changed from an unsaturated state to a saturated state, the pore water pressure and soil pressure increased, and then the slope was damaged, both of which decreased. Under high rainfall intensity, the slope was damaged, the soil in the slope was rapidly saturated, and the time required to produce the sliding area was short. When the rainfall intensity was the same, the smaller the slope angle was, the smaller the safety factor was. When the slope angle was the same, the greater the rainfall intensity was, the smaller the safety factor was.

Keywords: rainfall; slope instability; soil deformation; model test; numerical simulation

check for updates

Citation: Sun, Y.; Yang, K.; Hu, R.; Wang, G.; Lv, J. Model Test and Numerical Simulation of Slope Instability Process Induced by Rainfall. *Water* **2022**, *14*, 3997. https://doi.org/10.3390/w14243997

Academic Editor: Xingwei Ren

Received: 14 November 2022
Accepted: 5 December 2022
Published: 7 December 2022

1. Introduction

Under the effect of rainfall over time, changes in the shear strength and matric suction of a slope lead to instability and failure, which can lead to landslides and other geological disasters [1–7]. More than half of the landslide disasters in China are caused by rainfall [8,9]. Therefore, it is of great significance to evaluate slope stability and take effective measures to reduce the frequency of landslides by studying the seepage field, slope deformation and failure process, and the changes in stress states after rain. Sun Y [10] summarized the effects of slope stability during rainfall. Various scholars have used the finite element seepage analysis [11–13], finite element strength reduction method [14–16] and limit equilibrium method [17–20] to analyze the stability of a slope under rainfall conditions. A large number of studies [21–24] analyzed the seepage field of internal moisture flow inside a slope during rainfall. Many authors [25–29] have studied the failure mechanism of slope instability after rainwater infiltration. Chen Shusheng [30] studied the impact of rainfall and groundwater on slope soil by using the finite element strength reduction method, and compared the results of the finite element strength reduction method with those of the limit equilibrium method. Augusto Filho, O [31] studied the stability analysis of unsaturated soil slope under the condition of unstable seepage, and analyzed the stability of the slope through finite element seepage analysis combined with the finite element strength reduction method and limit equilibrium method. A large number of studies [32–35] quantitatively described the coupling analysis of seepage and deformation of unsaturated soil through finite element analysis. Wang Y. X. [20] concluded through a numerical simulation that with the increase of rainfall infiltration intensity and time, the sliding failure surface of the slope tends to move to the shallow layer, and the safety factor will decrease. Many authors [36–41] analyzed the influence mechanism of soil anisotropy on slope stability under rainfall conditions and determined that the influence of soil anisotropy on stress levels cannot be ignored. Khan et al. [42] studied the mechanism of rainfall intensity on the seepage field, stress strain field and slope stability by combining an unsaturated slope hydraulic coupling theory and a numerical simulation method. Jing Xiaofei [43] considered the migration of the slope angle to the wetting front under rainfall conditions, and studied, in depth, the influence of slope angle on the rainfall slope. Wang Shuhong [44] determined from ABAQUS that the change in slope stability during rainfall is mainly controlled by upstream cracks. Li Gang et al. [45–47] applied a strength reduction method to analyze and calculate the slope internal seepage during rainfall conditions and simulated the natural engineering of slope instability and construction excavation.

From a review of the current research, there is little research on slope failure mechanism and internal stress state of slope soil under rainfall. Therefore, it is necessary to further carry out model tests of rainfall infiltration on slope stability and carry out corresponding numerical simulation analyses and verification. In this study, through an indoor model test and geo-studio simulation method, the stability of a slope affected by rainfall was analyzed. The variation law of phreatic line, seepage field, the most dangerous sliding surface, and safety factor over time were also studied under rainfall infiltration, and the failure process of a slope under rainfall was analyzed.

2. Slope Model Test Design

2.1. Device for Slope Model Test under Rainfall

For the research on slope instability and failure, in view of the shortcomings of imperfect theoretical research and long prototype test cycle and high cost, a simple and intuitive small-scale conventional mechanical model test was developed in a relatively short time period and has gradually become a reliable research method.

A model test box of $2.0 \times 1.0 \times 1.2$ m was selected for testing the change in water level of the slope under the effect of rainfall, and a grid with a spacing of 10 cm was drawn on the side wall to monitor the deformation and damage of the slope. PVC pipes were set up in 11 rows at the top to simulate the rainfall process, and four 20 mm round holes were cut out at the front of the box.

2.2. Slope Fabrication and Instrument Burial

The process of making the physical model used in this test is described as follows:

(1) A layered filling method was used to make the slope;
(2) Before layered filling, roughen the whole layer;
(3) A rubber stopper sign was embedded at the designed lateral deformation monitoring point;
(4) The earth pressure box was placed at the pre-designed layer with the help of a PVC pipe, then backfill and tamp it;
(5) The fully filled seepage meter was placed at the pre-designed seepage scoring layer with the help of a PVC pipe and backfill and tamp it;
(6) A scraper was used to form the slope shape required for the test and an inverted filter layer was laid in front of the slope, so as to eliminate seepage water;
(7) The ring knife sampling method was used to test the slope soil samples after filling. Table 1 shows the parameters obtained in the model test. Figure 1 shows the layered filling of the slope, and Figure 2 shows the layout of the marking points.

Table 1. Physical and mechanical parameters of soil mass.

Soil	Test Weight γ (kN/m^3)	Permeability Coefficient k (cm/s)	Cohesion c (kPa)	Friction Angle φ (°)
Silt	23.0	1.9×10^{-4}	1.92	23

Figure 1. Model slope fabrication.

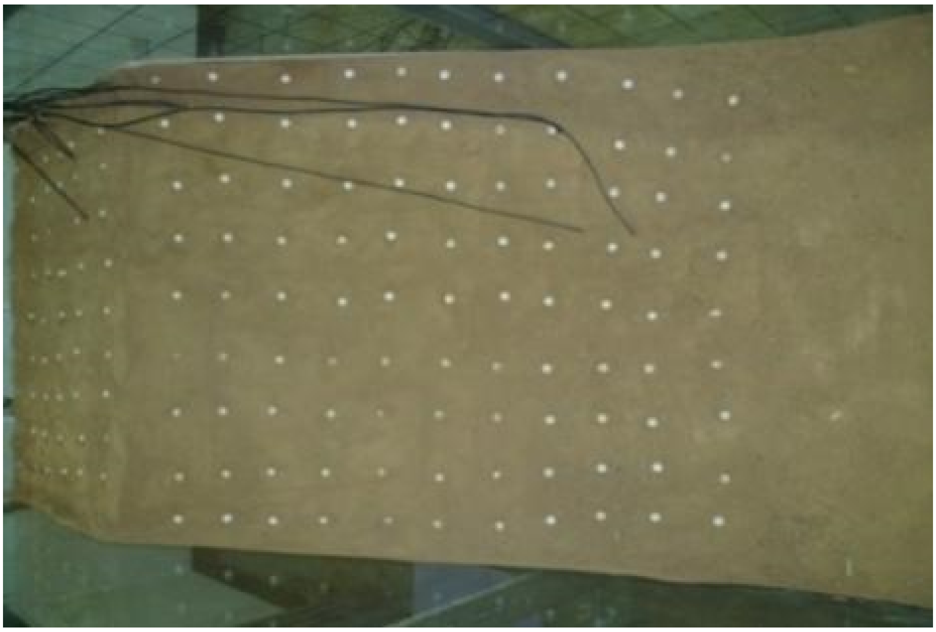

Figure 2. Slope sign layout.

In order to mitigate the influence of the placed sensors on the seepage field and stability of the slope, the instrument was buried at different positions in layers. The origin point was the right side of the box on the model, the left direction represented the x-axis, the inward direction was the y-axis, and the upward direction was the z-axis. The earth pressure box was embedded at: a (0.4, 0.4, 0.2), b (0.3, 0.4, 0.5), and c (0.2, 0.4, 0.8); while the osmometer was embedded at: a (0.4, 0.5, 0.2), b (0.3, 0.5, 0.5), and c (0.2, 0.5, 0.8).

3. Mechanism and Result Analysis of Model Test

3.1. Failure Mechanism of Slope under Rainfall

Different rainfall intensities had different effects on slope stability. The rising speed of the phreatic line in the slope increased with an increase in the accumulated seepage water, and the displacement change in the slope was more pronounced. When under rainfall, the time of slope deformation and instability was advanced. The greater the rainfall intensity, the higher the infiltration line was on the slope, and the slope coefficient decreased with time. The deformation process was divided into four stages: the displacement increased gradually; basic stability of displacement; small changes; and destruction.

Under prolonged rainfall, the rainwater would infiltrate the model slope through the broken surface. The amount of water that had not been discharged increased, making the phreatic line in the slope rise. The total pressure of the overlying soil and water continuously increased, increasing the water pressure acting on the potential sliding surface of the slope. At a certain point, the super hydrostatic pressure in the slope increased sharply, the shear strength of the slope dropped suddenly, and the slope was damaged. The permeability coefficient of silt was small, and it took a long time for rainwater to penetrate to the bottom of the slope. At this point, the upper soil mass of the slope was nearly saturated, and constantly collapsing due to the rainfall. With the accumulation of time, the phreatic line in the slope rose, gravitational cracks appeared on the top of the slope and became wider under the action of rainfall, forming the phenomenon of sliding soil. The water greatly reduced the strength of the soil at the foot of the slope. The sliding surface area continuously developed from the toe to the top of the slope, causing cracks under stress, and finally the slope was damaged as a whole.

3.2. Characteristics of the Pore Water Pressure and Earth Pressure

Figure 3 shows the change in pore water pressure in the slope under rainfall.

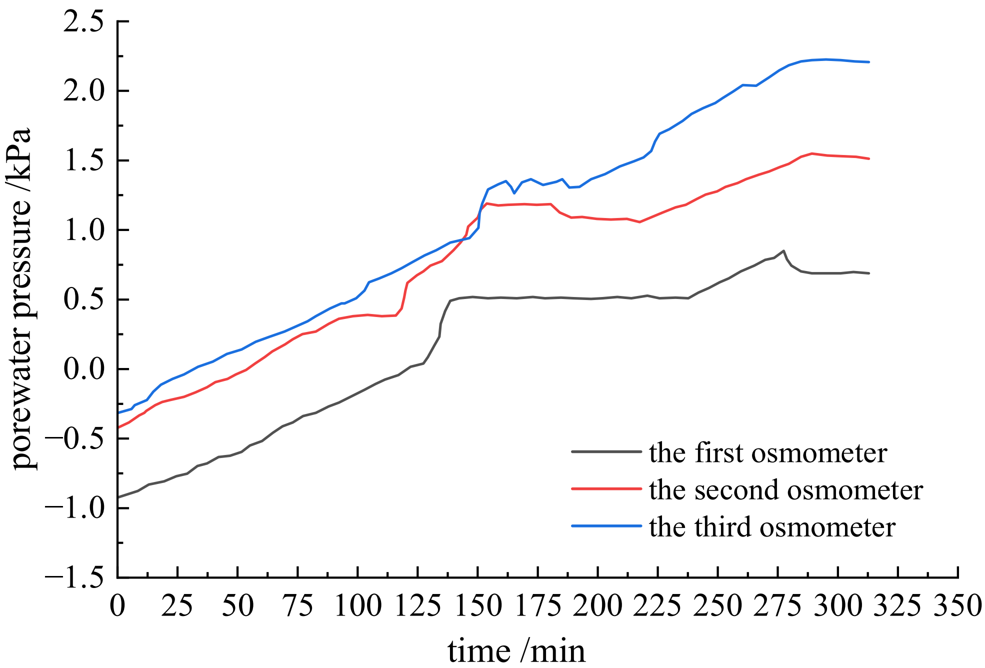

Figure 3. Change in pore water pressure in the slope under rainfall.

At 36 mm/h rainfall intensity, the pore water pressure acting on the potential sliding surface of the slope increased, and the readings from the osmotic pressure gauge buried in the slope also increased. The phreatic line in the slope continued to rise. Since the phreatic line was the boundary between saturated and unsaturated soil, the permeability meter reading at the lower part of the slope was greater than that at the upper part. When the entire slope soil mass was saturated, the reading on the osmometer stabilized. When the slope was damaged, the water in the slope was partially drained, and the reading of the osmometer dropped.

Figure 4 shows the change in soil pressure inside the slope during rainfall.

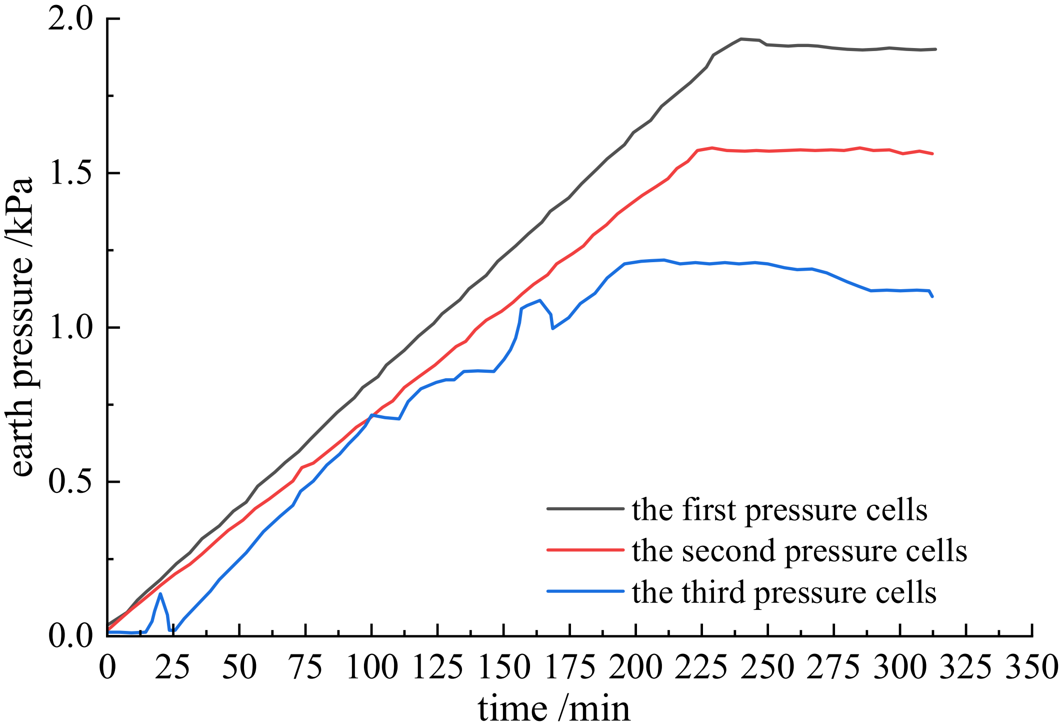

Figure 4. Change in soil pressure inside the slope during rainfall.

At a rainfall intensity of 36 mm/h, the pressure on the soil mass increased, and the readings on the buried earth pressure box also increased. When the slope was saturated, the reading of the earth pressure box was stable. After the slope stability reached a critical stable state, the slope was damaged, the reading on the earth pressure box decreased, and the sliding soil accumulated at the foot of the slope to form a new gentle slope; this prevented the slope from sliding further thereby increasing the overall shear strength of the slope.

4. Analysis of Numerical Simulation

The change in situation of the pore water pressure and earth pressure in the slope throughout the model test under rainfall was studied. We conducted the related numerical simulation study to analyze the phreatic line, seepage field, safety factor, and variation of sliding surface inside the slope.

The slope was studied through the numerical simulation analysis using the geo-studio software in this paper. The variations of the phreatic line, seepage field, the most dangerous sliding surface, and safety factor over time in the slope were studied.

Slope size, rainfall intensity, and soil parameters of the numerical simulation were the same as that of the experimental slope. The size of the slope is shown in Figure 5. Figure 6 shows the grid distribution of the model.

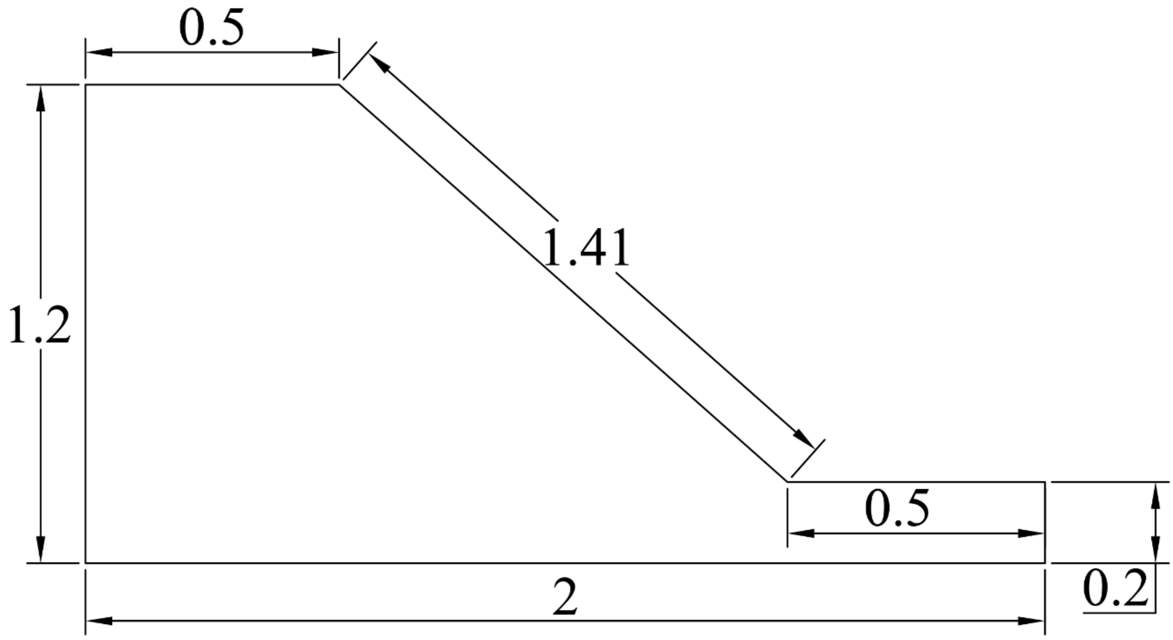

Figure 5. Size of slope.

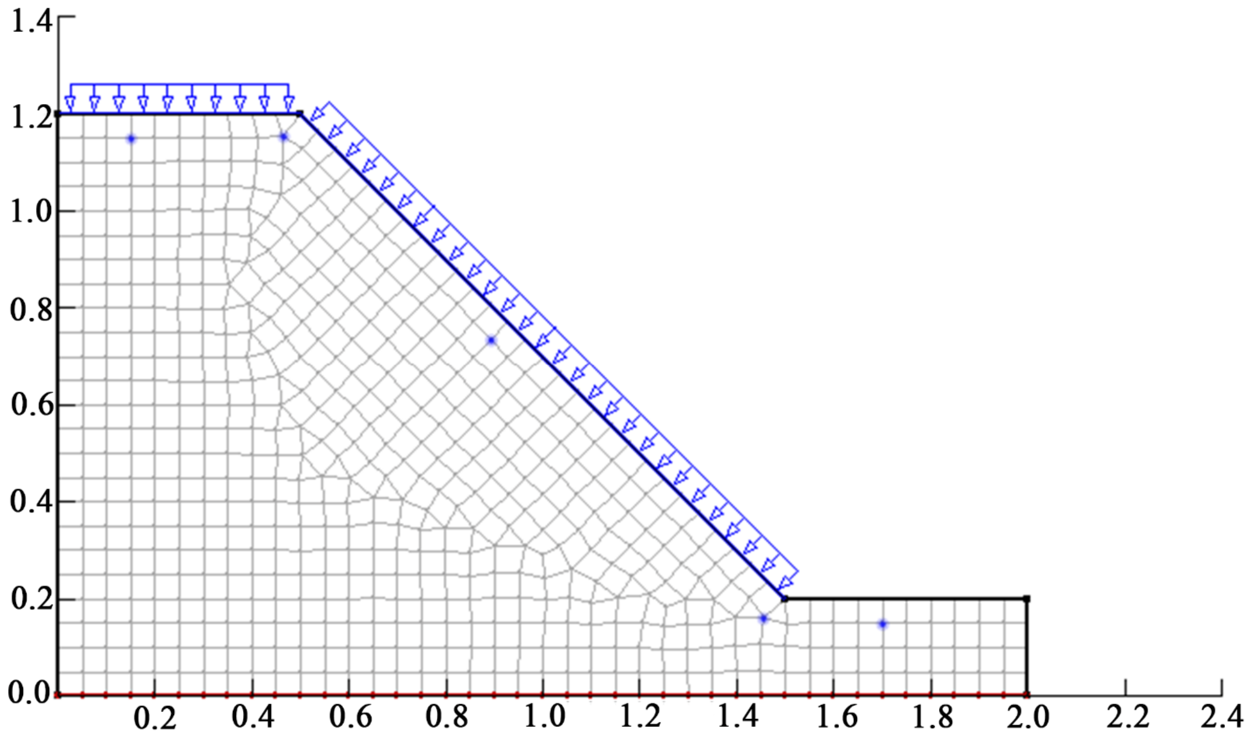

Figure 6. Grid distribution of the model.

The initial conditions of transient seepage in the slope were described by distributions of pore water pressure, soil moisture, and matric suction. Under a natural state, the seepage field had a great impact on the count of the saturated-unsaturated results. The bottom of the slope was at a pressure of zero head, the soil was unsaturated, and the steady seepage field distribution was calculated under the rainfall.

Figure 7 shows the hydraulic conductivity function at a permeability coefficient of 1.9×10^{-4} m/s. When the pressure was negative, the moisture of the soil became unsaturated, and the moisture content was reduced. The smaller the negative pore water pressure of soil, the greater the soil ability to transmit the water pressure.

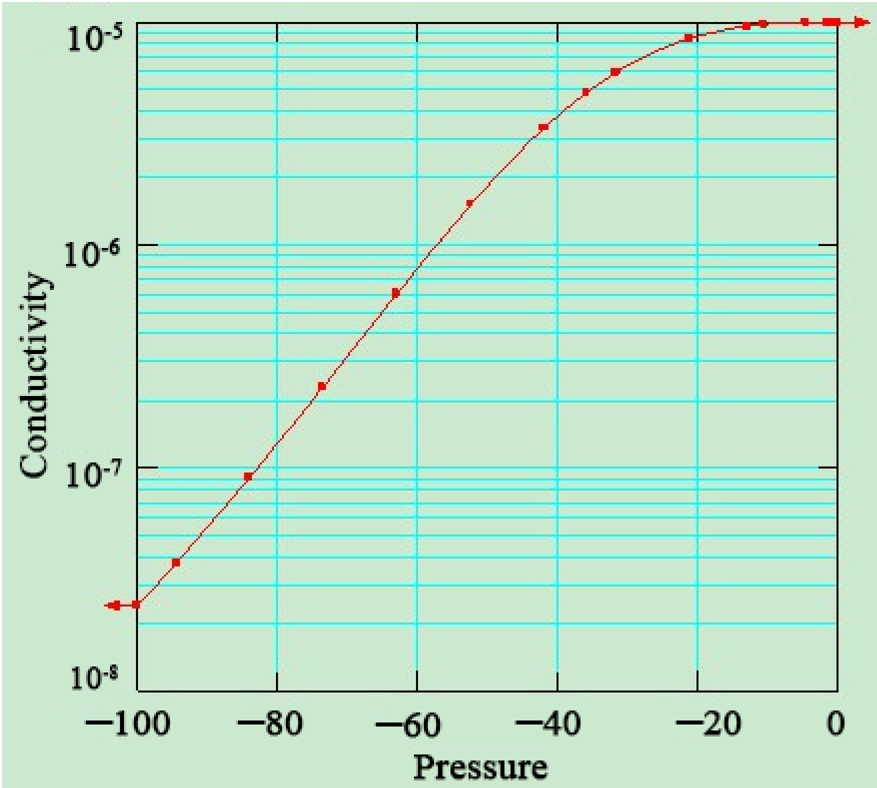

Figure 7. Hydraulic conductivity function at a permeability coefficient of 1.9×10^{-4} m/s.

The volume water content function depresses the water volume inside the soil under the influence of the pore water pressure. When the pore water pressure became negative, the soil became unsaturated, and the volume water content began to drop. The content of the soil material was defined as the volume water content, which is a product of porosity and saturation of the soil. The formula is as follows:

$$\Theta = nS_r \tag{1}$$

where Θ is the volume water content, n is the porosity, and S_r is the saturation.

Figure 8 shows the volumetric moisture content. The negative pore water pressure and volumetric moisture content were positively correlated, and under low negative pore water pressure, the growth rate of volume water content is large.

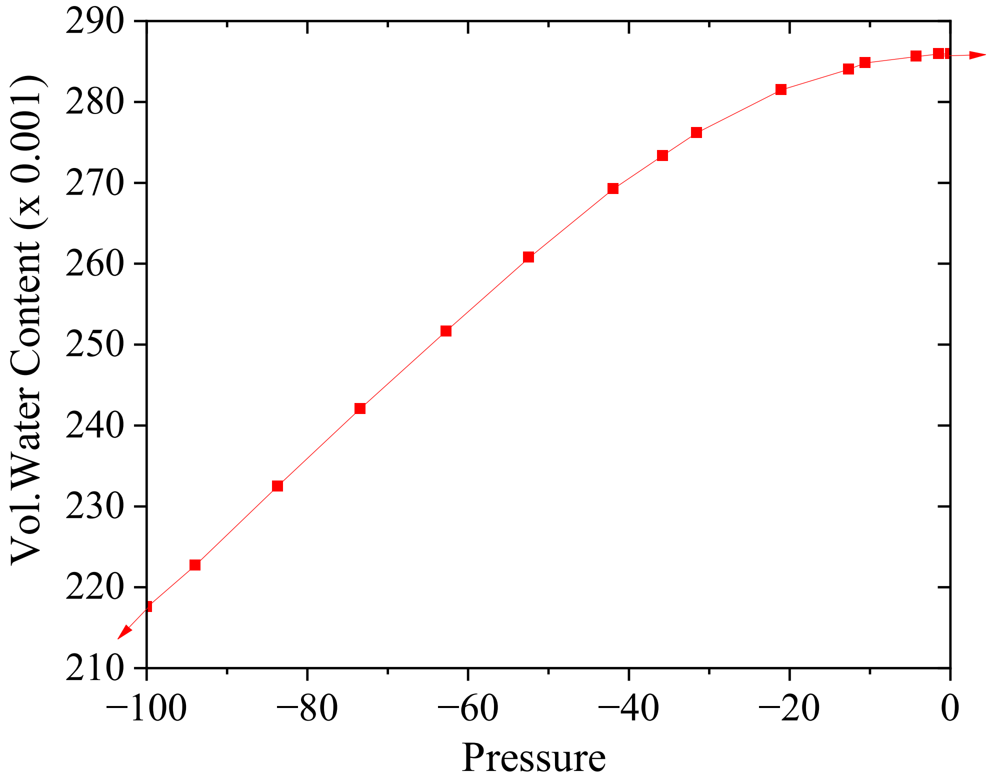

Figure 8. Volumetric moisture content.

4.1. Seepage of the Slope at All Times

Figures 9–12 show changes of the slope phreatic line and seepage field after 1, 2, 3, and 4 h of rainwater infiltration.

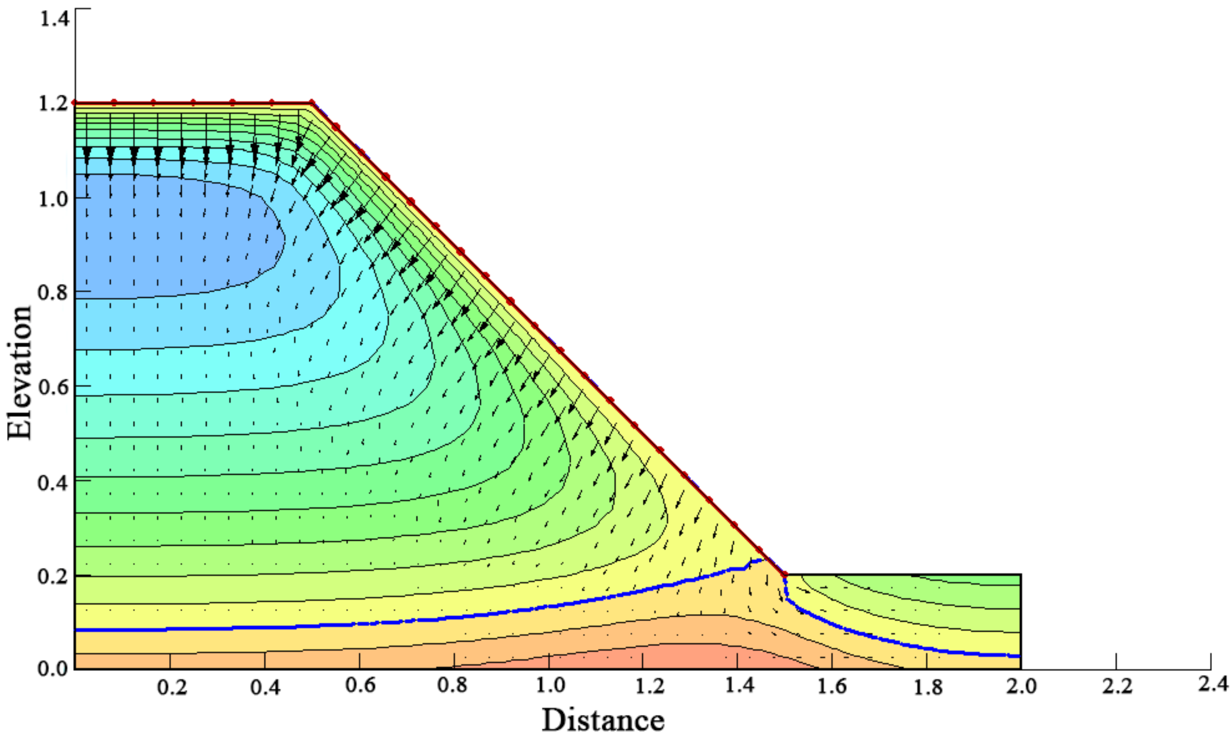

Figure 9. Changes of the slope phreatic line and seepage field after 1 h of rainwater infiltration.

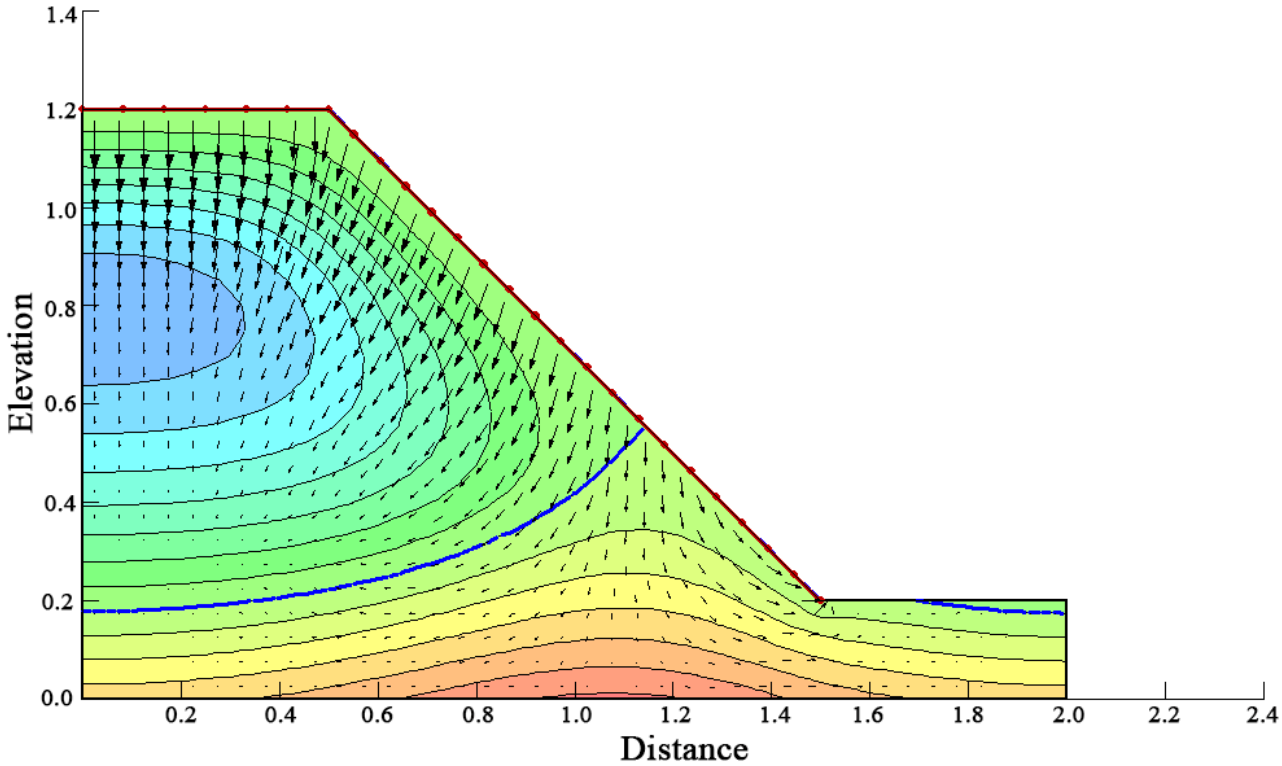

Figure 10. Changes of the slope phreatic line and seepage field after 2 h of rainwater infiltration.

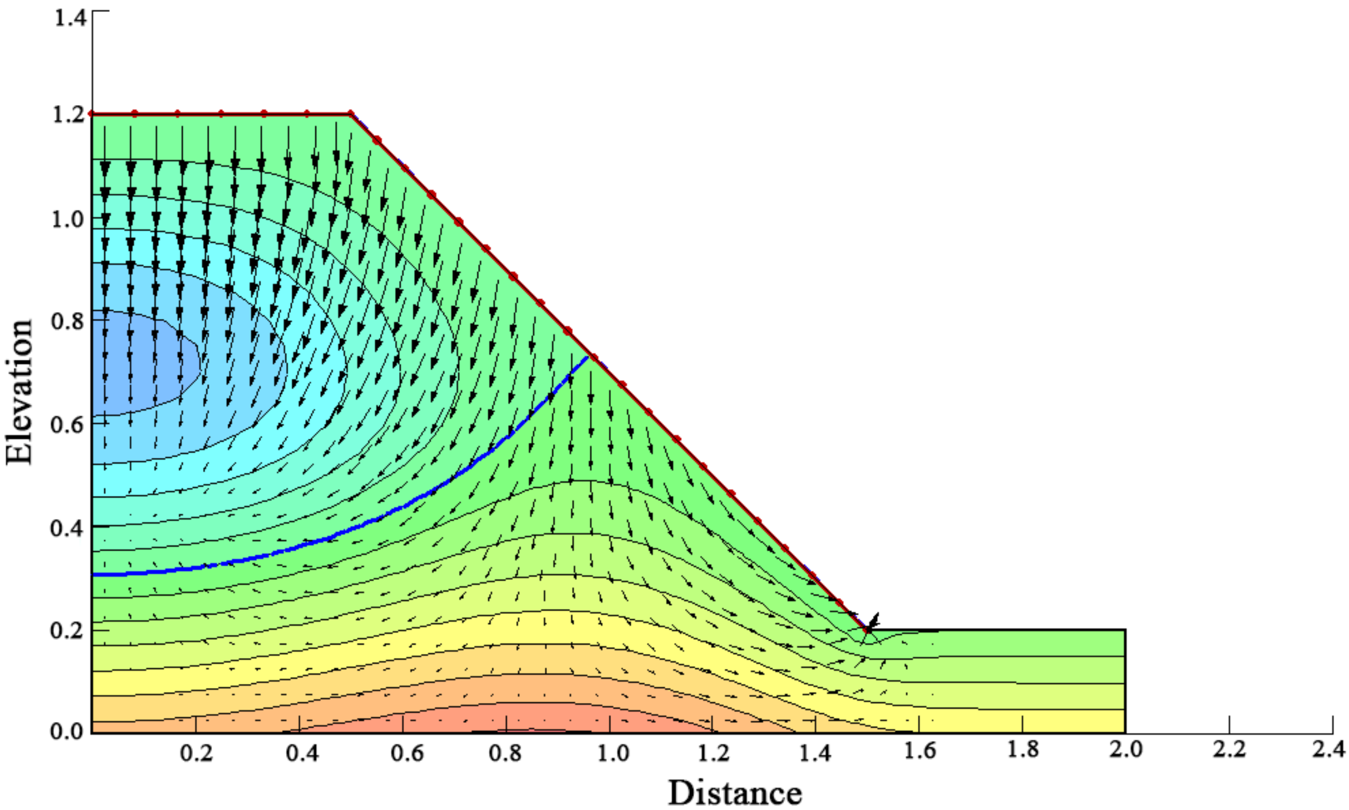

Figure 11. Changes of the slope phreatic line and seepage field after 3 h of rainwater infiltration.

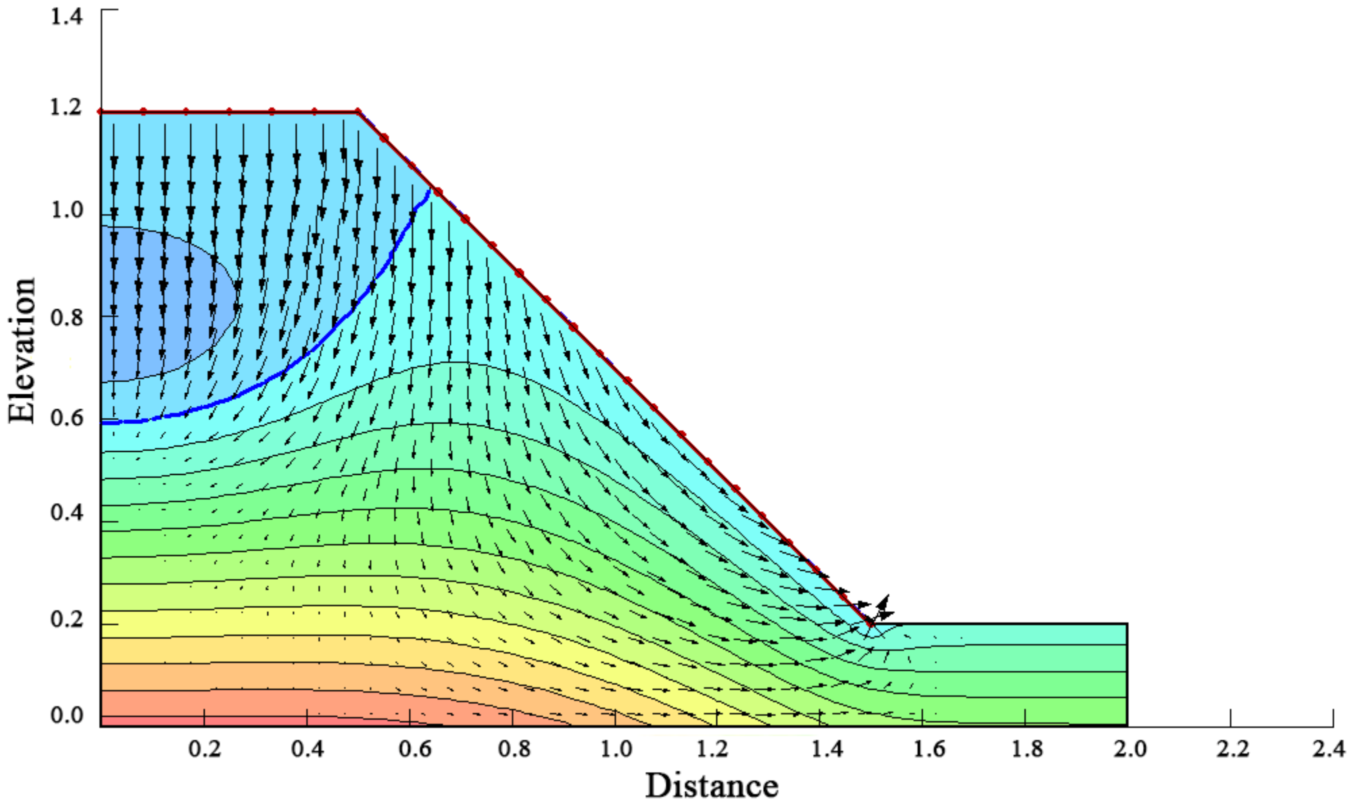

Figure 12. Changes of the slope phreatic line and seepage field after 4 h of rainwater infiltration.

The seepage at 1 h at an intensity of 36 mm/h is shown in Figure 9. The arrows indicate the direction of rainfall infiltration, the colored areas represent the water head equipotential line, and the blue line represents the phreatic line of the water level. The arrows become smaller from the slope surface to center, and finally disappear at the slope center, with a water head height of about 0.08 m. The water head increased gradually from left to right on the slope, the width of its equipotential line gradually decreased, the phreatic line under an intensity of 36 mm/h inside the slope was about 0.2 m, the maximum water head at an intensity of 36 mm/h was below the phreatic line, and the location of minimum water head was between 0.78 m and 1.05 m. We can draw some conclusions through the analysis. The direction of infiltration was perpendicular to the slope surface, the seepage velocity decreased from the slope surface to the interior, there was no infiltration at 0.08 m, some water flowed into the slope, and some water flowed along the surface of slope to the location of the phreatic line. There was unsteady seepage above the phreatic line, there was steady seepage below the unsteady seepage, the infiltration speed was the largest, the water head was the largest, and the water head mainly stayed on the surface of the slope. Under rainfall conditions, the seepage level rose within 1 h, the water head continued to increase during the rainfall, the infiltration depth in the slope increased, unsteady seepage occurred in the slope, and the anti-shear strength began to decrease.

The seepage in the slope after 2 h at 36 mm/h is shown in Figure 10. All arrows are distributed in the interior of the slope, and the arrows decrease in size from the slope surface to the center. The arrow density in Figure 10 is greater than that in Figure 9. The water head gradually dropped from the left side of slope to the right, the width of the water head equipotential line decreased gradually, the width of the slope center in Figure 9 is smaller than that in Figure 10, and the arrows are nearly parallel with the surface of the slope and the base of slope below the phreatic line. The location of the phreatic line was 36 mm/h on the surface of a slope that was approximately 0.5 m. The location of the maximum water head at 36 mm/h was below the phreatic line, and the location of the minimum water head was between 0.65 m and 0.9 m. The seepage occurred throughout the slope in 2 h, and the seepage from outside to inside the slope increased with time. There was unsaturated seepage above the phreatic line, the direction of seepage was perpendicular to the slope surface, the soil was saturated below the phreatic line, the direction of infiltration was parallel to the slope surface and bottom, the seepage downward sharply approached the phreatic line. The width of the water head equipotential lines was more uniform than that of the 1 h case, the curvature of the water head equipotential lines decreased, the width of the water level equipotential lines at low water heads was larger than that at high water heads. The unsteady infiltration was obvious in unsaturated and saturated areas, and the stability of the slope was poor. Some conclusions can be drawn from the analysis. The position of the phreatic line rose after 2 h of rainfall, the water head increased continually with rainfall, the infiltration depth in the slope increased, unstable seepage occurred inside the slope, and the shear strength started to decrease. The slope had poor stability and tended to slide.

The seepage in the slope after 3 h at an intensity of 36 mm/h is shown in Figure 11. The phreatic line was higher after 3 h than after 2 h. The arrows were intensive at the top of the slope, the arrows were perpendicular to the inside of the slope first, then the arrows had a defined angle with the left border, and the width of the colored area increased gradually. The maximum water head at 36 mm/h was located at the bottom of the slope, and the minimum water head in the slope was between 0.62 and 0.82 m. The maximum and minimum water heads changed on the slope surface, but the minimum water head changed dramatically. The direction of infiltration was perpendicular to the slope surface above the phreatic line and nearly parallel to the slope surface and bottom. There was steady infiltration according to the analysis in 3 h. There were steady infiltration and unsteady infiltration in the slope in 3 h. The unsteady infiltration above the phreatic line in the slope was more obvious, the reaction between the water and soil was stronger, the infiltration rate was greater, the stability of the slope was poor, and the anti-shear strength decreased sharply.

The seepage inside the slope within 4 h at an intensity of 36 mm/h is shown in Figure 12. The infiltration is distributed over the surface of the slope, the phreatic line is located between 0.6 m and 1.0 m, and the arrows were perpendicular to the slope surface at the top of the slope. The direction of infiltration was nearly parallel with slope surface and slope bottom. The arrows were increasingly coarse, the infiltration speed of the analysis was large, the equipotential lines were perpendicular to the surface of the slope and distributed evenly, the location of the maximum water head was at the bottom of the slope, and the location of the minimum water head was between 0.67 and 0.98 m.

Changes in the slope soil mass occurred over time in the analysis. First, the phreatic line rose inside the slope, and finally reached the top of the slope. Second, some rainwater slid along the sliding slope surface, while the rest seeped into the slope soil. There was unsteady seepage above the slope phreatic line, and the direction of the seepage was perpendicular to the slope surface. There was steady seepage below the slope surface. Due to the saturated state of the slope's soil, the seepage direction was parallel to the slope surface or bottom. When the seepage direction approached the phreatic line, it turned sharply downwards. Third, the water head height gradually decreased from the slope's left boundary to the right boundary. Water head width decreased gradually. Finally, after some time, the seepage overflow point of the slope became higher. The overflow surface of the slope increased in size, the phreatic line of the slope increased in height, the water head increased, the seepage depth in the slope increased, and the slope stability worsened.

4.2. Variation of Slope Stability with Rainfall Time

Figures 13–16 show the change in safety factor and potential sliding surface of the slope under rainfall infiltration, over periods of are 1, 2, 3, and 4 h. The most dangerous sliding surface was computed through the slope/w over each period, and the minimum safety factor was found to be 1.075, 0.994, 0.928, and 0.860 for 1, 2, 3 and 4 h, respectively. A safety factor of 1 or above indicates that the slope is stable.

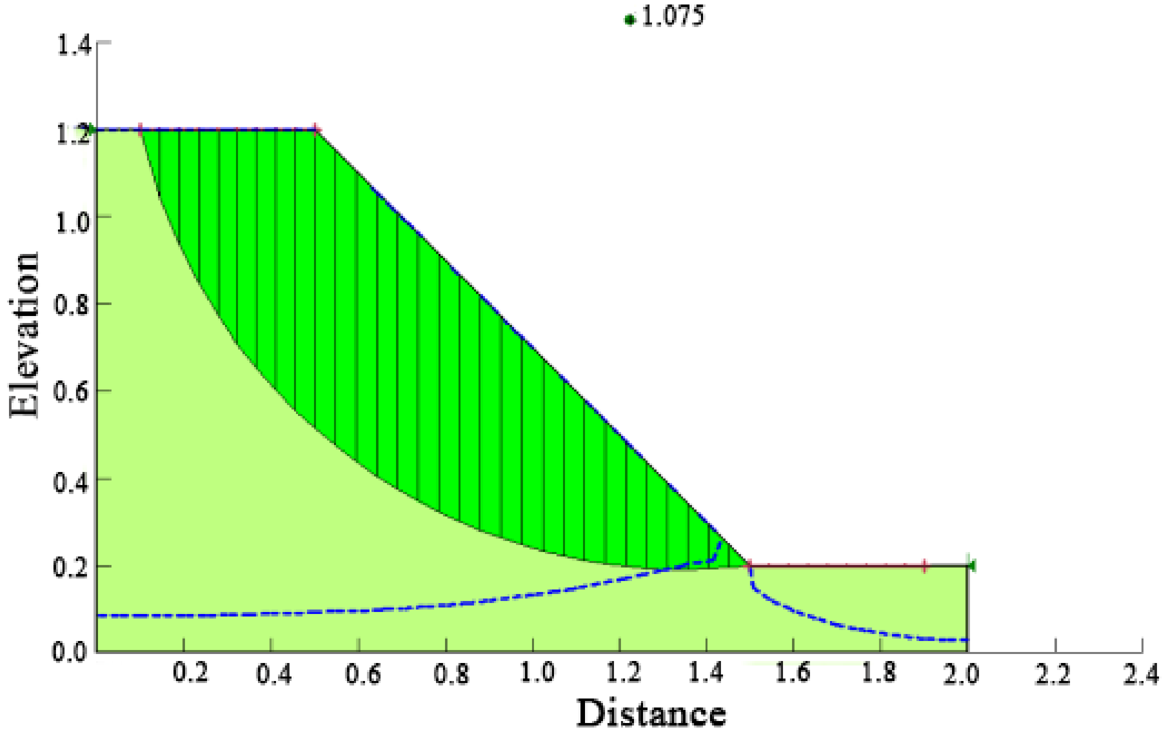

Figure 13. The slope sliding surface in 1 h.

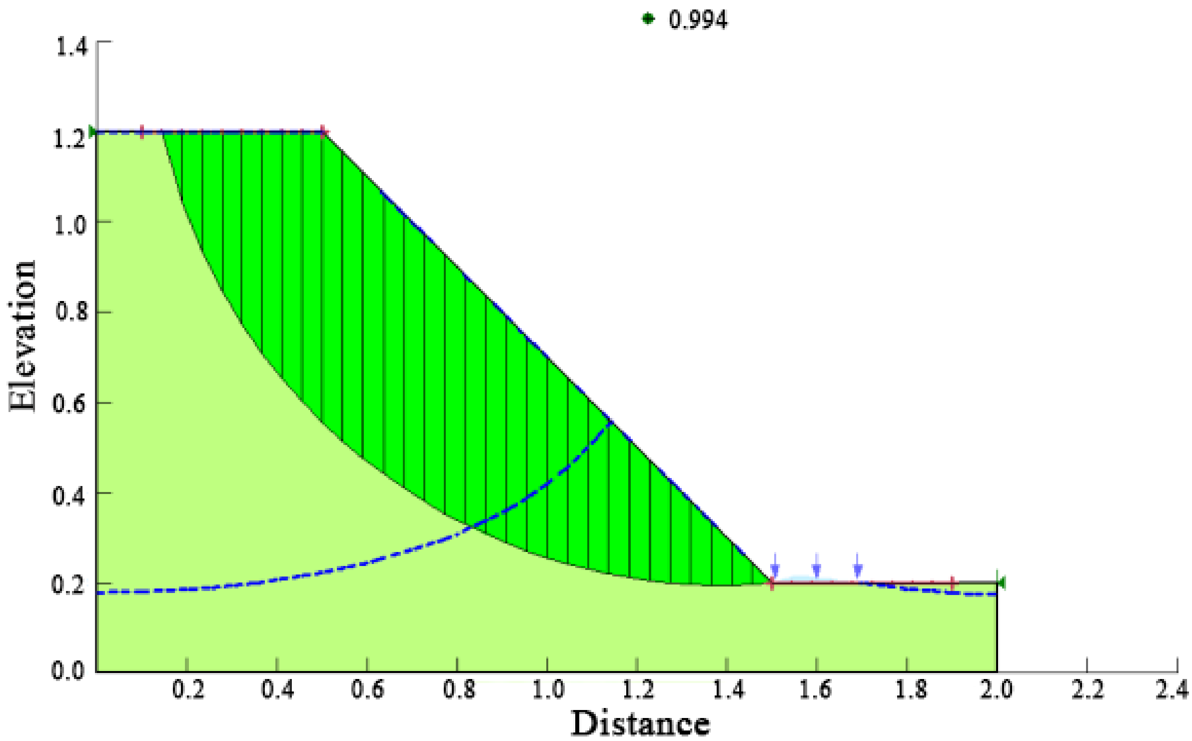

Figure 14. The slope sliding surface in 2 h.

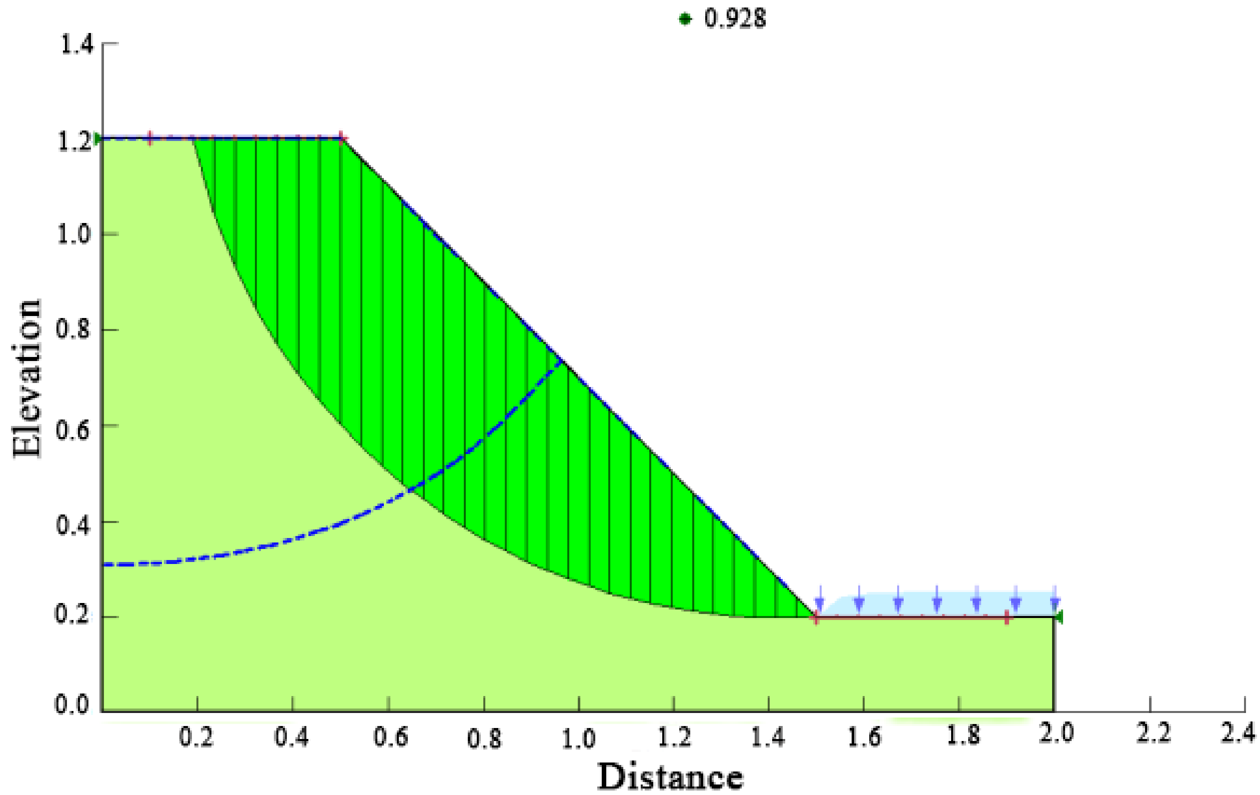

Figure 15. The slope sliding surface in 3 h.

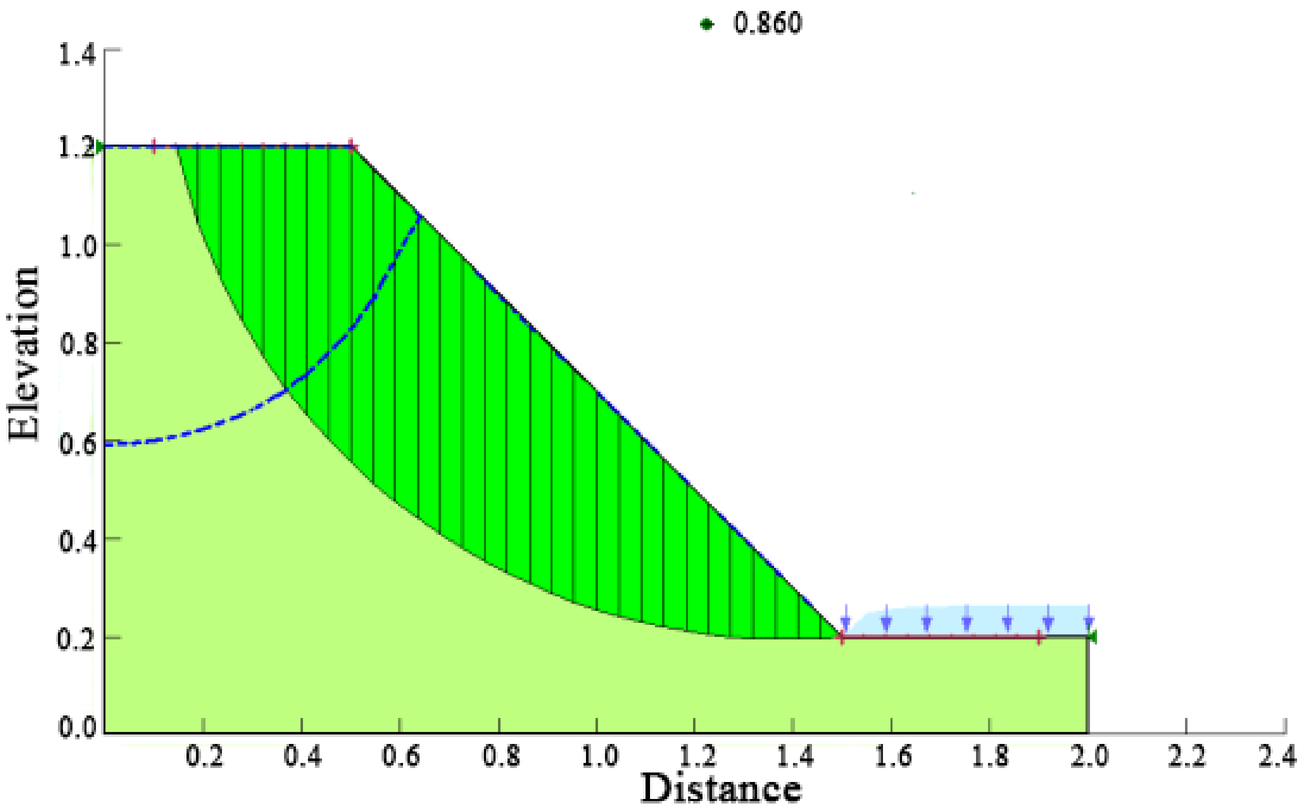

Figure 16. The slope sliding surface in 4 h.

Figure 17 shows that during rainfall, the safety factor of the slope decreased over time. After 2 h, the slope safety factor was less than 1, which indicates that the slope was damaged.

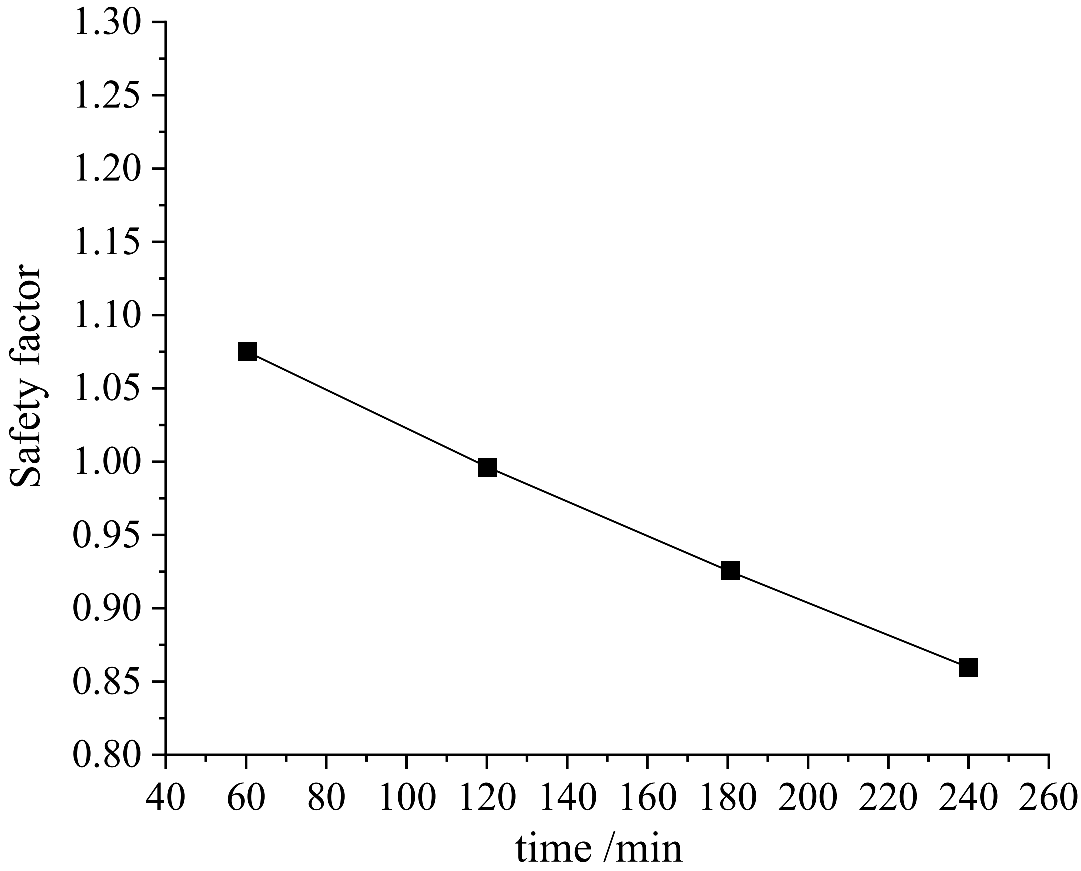

Figure 17. The diagram of safety factor under different time under rainfall.

The curve of the slope safety factor indicates many things at different times under rainfall. The safety factor and stability decreased with rainfall. The slope safety factor decreased, the speed of safety factor did not noticeably decrease, and the stability of the slope stabilized. There are a number of possible causes for the change. The water had an effect on the soil due to hydrostatic and hydrodynamic pressure. This made the potential slip surface or slip zone slide through the softened soil. The soil shear strength decreased rapidly, and the internal friction angle was close to 0. Even if the angle of the slope was small, the slope could still slide. The downward sliding force of the slope was increased by the hydrostatic and hydrodynamic pressure. The slope shear strength decreased, and the water content increased in unsaturated soil by rainfall infiltration. The matric suction inside the soil decreased rapidly, the shear strength decreased, the slope safety factor decreased, and the slope was unstable and consequently damaged.

4.3. Analysis of the Failure Mode of Slope Instability

During rainfall, the slope failure presented a typical traction development mode. With continuous rainfall, rainwater seeped into the slope, and when the water level in the slope rose, the lower soil layer was subjected to the pressure from the upper soil layer, the stress and displacement of the soil layer inside the slope gradually reached a critical state, and the slope was eventually damaged. During the downward sliding of the slope soil mass, the sliding soil mass accumulated at the foot of the slope to form a gentle slope, which increased the slope shear strength. The shape of the sliding surface after the test is shown in Figure 18. A series of the most dangerous sliding surfaces at different times were also obtained through numerical simulation according to the phreatic line at each time. The shape of the sliding surface obtained from the test was consistent with that obtained from the software simulation, as shown in Figures 16 and 18.

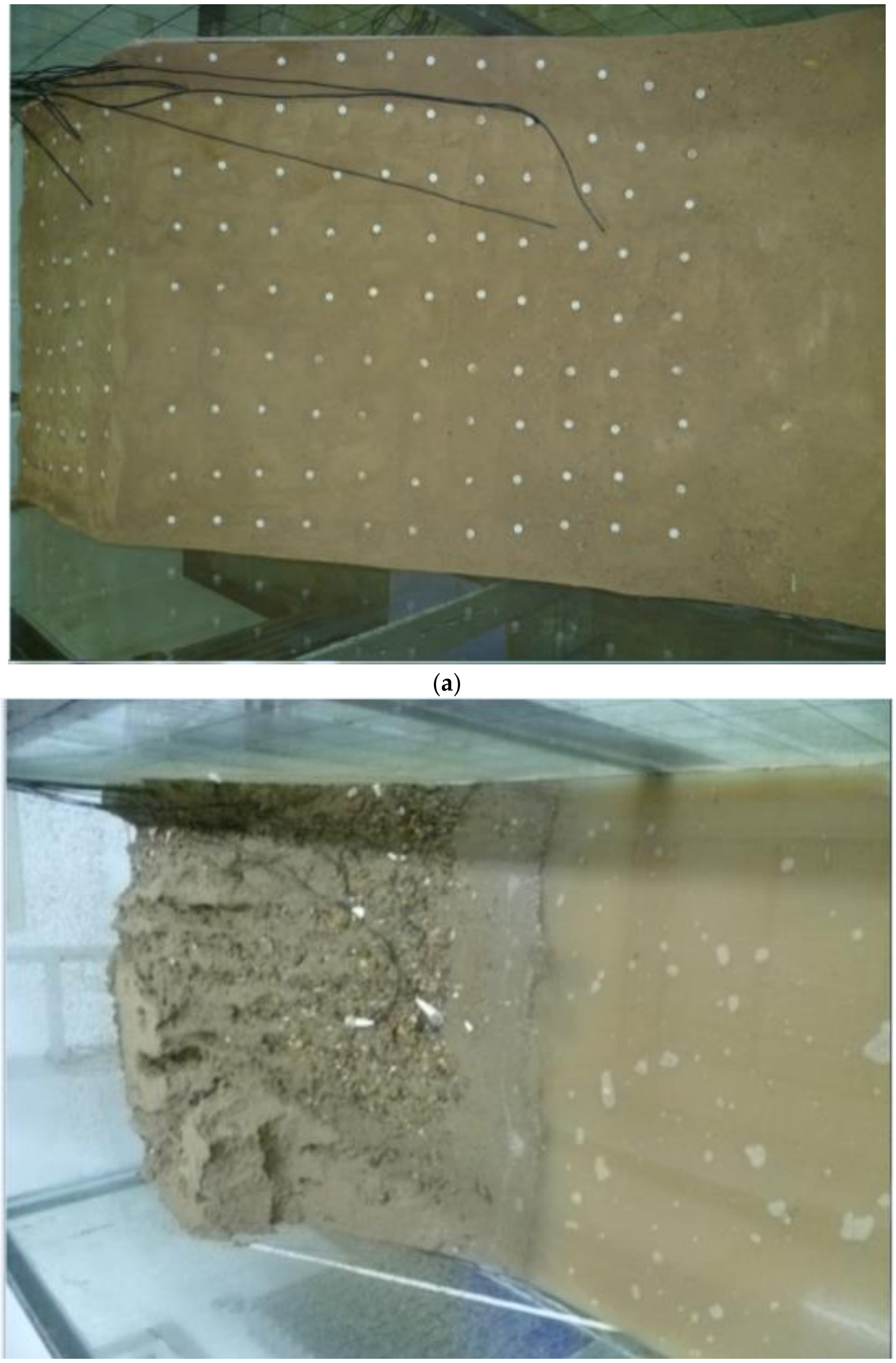

(**a**)

(**b**)

Figure 18. The slope sliding surface of the test: (**a**) the sliding surface of test at initial time; (**b**) failure mode of sliding surface at the end of slope.

5. Discussions and Conclusions

In this study, through a model test and geo-studio simulation method, the variation law of phreatic line, seepage field, the most dangerous sliding surface, and safety factor over time was studied under rainfall infiltration, and the failure process of a slope under rainfall was analyzed.

i. During rainfall, the slope failure presented a typical traction development mode. As the rainfall continued, the rainwater seeped into the slope, the water level in the slope rose and caused the displacement of the soil mass to gradually increase to the critical stable state. The soil layer at the back edge of the slope was damaged, and the sliding soil accumulated at the foot of the slope, forming a gentle slope, which increased the slope shear strength, making the slope finally reach a stable state;
ii. With the increase in rainfall over time, the phreatic line rose in the slope and finally reached the top of the slope. Some rainwater slid along the sliding surface of the slope, while the remaining infiltrated into the slope soil. There was unstable seepage above the phreatic line of the slope. The seepage direction was perpendicular to the slope surface, while the seepage direction was parallel to the surface or slope bottom. When the seepage direction was close to the phreatic line, it dropped sharply. The water head height decreased gradually from the left boundary to the right boundary of the slope, and the water head width decreased gradually. Over time, the phreatic line of the slope kept rising, the water head kept increasing, the seepage depth inside the slope became deeper, and the slope stability worsened until the slope was damaged. Then, the phreatic line of the slope decreased, and the pore water pressure decreased. In this process, the overburdened soil changed from the unsaturated to the saturated state, and the earth pressure value increased, followed by slope failure, after which the earth pressure value decreased;
iii. Under high rainfall intensity, the slope was damaged, the soil in the slope was rapidly saturated, and the time required to produce the sliding area was short. The drainage condition was limited by high rainfall. If the soil strain was large at this time, the excess pore water pressure of the soil would be elevated, causing slope failure. Under the action of high rainfall intensity, the slope is more vulnerable to sliding failure;
iv. According to the geo-studio numerical calculation results, when the rainfall intensity was kept constant, having smaller slope angles resulted in smaller safety factors. When the slope angle was kept constant, the greater rainfall intensity lead to smaller safety factors;
v. Due to the restriction of the experimental conditions and time, various safety factors affecting slope stability could not be studied. Only the model test of a slope under rainfall was studied, and the centrifugal model test corresponding to the effects of rainfall infiltration on a slope remains an area of further study. It was necessary to ensure that the experimental data corresponded with the analysis and validation of the numerical simulation.

Author Contributions: Author Contributions: Conceptualization, R.H. and G.W.; Methodology, J.L.; Software, K.Y.; Validation, J.L.; Formal analysis, G.W.; Investigation, R.H.; Resources, G.W.; Data curation, K.Y.; Writing—original draft, Y.S.; Writing—review & editing, Y.S.; Visualization, K.Y. and J.L.; Project administration, K.Y., R.H. and G.W. All authors have read and agreed to the published version of the manuscript.

Funding: This work is supported by the Beijing Natural Science Foundation (8214060), National Natural Science Foundation of China (42107164).

Institutional Review Board Statement: Not applicable.

Informed Consent Statement: Informed consent was obtained from all subjects involved in the study.

Data Availability Statement: All data that support the findings of this study are available from the corresponding author upon reasonable request.

Acknowledgments: This work is supported by the Beijing Natural Science Foundation (8214060), National Natural Science Foundation of China (42107164). All authors have agreed to publish.

Conflicts of Interest: The authors declare no conflict of interest.

References

1. Wang, G.; Sassa, K. Factors affecting rainfall-induced flowslides in laboratory flume tests. *Geotechnique* **2001**, *51*, 587–599. [CrossRef]
2. Wang, H.; Jiang, Z.; Xu, W.; Wang, R.; Xie, W. Physical model test on deformation and failure mechanism of deposit landslide under gradient rainfall. *Bull. Eng. Geol. Environ.* **2022**, *81*, 66. [CrossRef]
3. Bao, C.; Zhan, L.; Xia, Y.; Huang, Y.; Zhao, Z. Development Trend and Stability Analysis of Creep Landslide With Obvious Slip Zone Under Rainfall-Taking Xinchang Xiashan Basalt Slope as an Example. *Front. Earth Sci.* **2022**, *9*, 808086. [CrossRef]
4. Chen, H.; Qin, S.; Xue, L.; Xu, C. Why the Xintan landslide was not triggered by the heaviest historical rainfall: Mechanism and review. *Eng. Geol.* **2021**, *294*, 106379. [CrossRef]
5. Roccati, A.; Faccini, F.; Luino, F.; Ciampalini, A.; Turconi, L. Heavy Rainfall Triggering Shallow Landslides: A Susceptibility Assessment by a GIS-Approach in a Ligurian Apennine Catchment (Italy). *Water* **2019**, *11*, 605. [CrossRef]
6. Nie, W.; Feng, D.; Lohpaisankrit, W.; Li, C.; Yuan, J.; Chen, Y. A dynamic Bayesian network-based model for evaluating rainfall-induced landslides. *Bull. Eng. Geol. Environ.* **2019**, *78*, 2069–2080. [CrossRef]
7. Li, W.L.; Zhu, J.; Fu, L.; Zhu, Q.; Xie, Y.K.; Hu, Y. An augmented representation method of debris flow scenes to improve public perception. *Int. J. Geogr. Inf. Sci.* **2021**, *35*, 1521–1544. [CrossRef]
8. Gao, Y.; Zhao, S.; Deng, J. Developing Law of Damming Landslide and Challenges for Disaster Prevention and Mitigation in the Three-river-parallel Territory in the Tibetan Plateau. *Adv. Eng. Sci.* **2020**, *52*, 50–61.
9. Guo, Y.; Yin, W. Study on the Development Situation of Disaster Discipline in China from the Perspective of Periodical Literature. *J. Catastrophol.* **2021**, *36*, 126–132.
10. Sun, Y.; Jia, C.; Wang, G. Overview of Research on Stability of Slope During Rainfall. *Constr. Technol.* **2012**, *41*, 4.
11. Deng, B.; Yang, M. Bearing capacity analysis of submerged slopes subjected to water drawdown based on a nonassociated flow rule and nonlinear failure criteria. *Bull. Eng. Geol. Environ.* **2021**, *80*, 835–850. [CrossRef]
12. Zhang, S.; Tang, H.; Liu, X.; Tan, Q.; Xiahou, Y. Seepage and Instability Characteristics of Slope Based on Spatial Variation Structure of Saturated Hydraulic Conductivity. *Earth Sci.* **2018**, *43*, 622–634.
13. Li, W.L.; Zhu, J.; Fu, L.; Zhu, Q.; Guo, Y.K.; Gong, Y.H. A rapid 3D reproduction system of dam-break floods constrained by post-disaster information. *Environ. Model. Softw.* **2021**, *139*, 104994. [CrossRef]
14. Yang, Q.; Li, R.; Zhang, S.; Li, R.; Bai, W.; Xiao, H. Algorithm Implementation of Equivalent Expansive Force in Strength Reduction FEM and Its Application in the Stability of Expansive Soil Slope. *Water* **2022**, *14*, 1540. [CrossRef]
15. Tao, Y.; Liang, W.; Xie, W. Research on the criterions of slope stability analysis based on finite element strength reduction method. *Ind. Constr.* **2019**, *49*, 103–106.
16. Liu, S.; Su, Z.; Li, M.; Shao, L. Slope stability analysis using elastic finite element stress fields. *Eng. Geol.* **2020**, *273*, 105673. [CrossRef]
17. Hsiao, D.H.; Hsieh, C.S.; Yeh, L.C.; Lin, D.Y.; Phan, V.T.A. A study on a instability slope in Taiwan subjected to rainfalls. In Proceedings of the 2nd International Conference on Sustainable Development in Civil, Urban and Transportation Engineering (CUTE), Ho Chi Minh, Vietnam, 17–19 April 2018.
18. Wei, Y.; Xia, M.; Ye, F.; Fu, W. Effect of drag force on stability of residual soil slopes under surface runoff. *Geomat. Nat. Hazards Risk* **2018**, *9*, 488–500. [CrossRef]
19. Taskiran, T.; Fidan, A.A. Investigation of the Parameters Affecting the Stability of Unsaturated Soil Slope Subjected to Rainfall. *TEKNIK DERGI* **2019**, *30*, 9483–9506. [CrossRef]
20. Wang, Y.; Chai, J.; Cao, J.; Qin, Y.; Xu, Z.; Zhang, X. Effects of seepage on a three-layered slope and its stability analysis under rainfall conditions. *Nat. Hazards* **2020**, *102*, 1269–1278. [CrossRef]
21. Li, S.; Jiang, Z.; Que, Y.; Chen, X.; Ding, H.; Liu, Y.; Dai, Y.; Xue, B. Water Field Distribution Characteristics under Slope Runoff and Seepage Coupled Effect Based on the Finite Element Method. *Water* **2021**, *13*, 3569. [CrossRef]
22. Shi, G.; Gu, G.; Zhou, H.; Tao, Z.; Pan, H.; Tang, T. Stability Monitoring and Analysis of High and Steep Slope of a Hydropower Station. *Geofluids* **2020**, *2020*, 8840269. [CrossRef]
23. Zhang, C.; Zhang, M.; Zhang, T.; Dai, Z.; Wang, L. Influence of intrusive granite dyke on rainfall-induced soil slope failure. *Bull. Eng. Geol. Environ.* **2020**, *79*, 5259–5276. [CrossRef]
24. Yue-ming, Z.; Dao-yong, G.; Ping-ping, L. Analysis of 3D saturated-unsaturated raining infiltration seepage. *J. Hydraul. Eng.* **2003**, *12*, 66–70.
25. Chen, L.; Zhang, X.; Pei, X.; Zhang, S.; Gong, W.; Zhong, Y. Model test of the linear loess fill slope instability induced by rainfall. *Hydrogeol. Eng. Geol.* **2021**, *48*, 151–160.
26. Wu, L.Z.; Zhang, L.M.; Zhou, Y.; Xu, Q.; Yu, B.; Liu, G.G.; Bai, L.Y. Theoretical analysis and model test for rainfall-induced shallow landslides in the red-bed area of Sichuan. *Bull. Eng. Geol. Environ.* **2018**, *77*, 1343–1353. [CrossRef]
27. Zeng, L.; Liu, J.; Shi, Z. Effect of colluvial soil slope fracture's anisotropy characteristics on rainwater infiltration process. *J. Traffic Transp. Eng.* **2018**, *18*, 34–43. [CrossRef]
28. Zhang, J.; Zhu, D.; Zhang, S. Shallow slope stability evolution during rainwater infiltration considering soil cracking state. *Comput. Geotech.* **2020**, *117*, 103285. [CrossRef]
29. Zhou, Z.; Zhang, J.; Ning, F.; Luo, Y.; Wang, J. Temporal and spatial characteristics of moisture migration and instability mechanism of cracked soil slope under rainfall infiltration. *J. Traffic Transp. Eng.* **2020**, *20*, 107–119.

30. Zhu, Y.L.; Ishikawa, T.; Zhang, Y.F.; Nguyen, B.T.; Subramanian, S.S. A FEM-MPM hybrid coupled framework based on local shear strength method for simulating rainfall/runoff-induced landslide runout. *Landslides* **2022**, *19*, 2021–2032. [CrossRef]
31. Augusto Filho, O.; Fernandes, M.A. Landslide analysis of unsaturated soil slopes based on rainfall and matric suction data. *Bull. Eng. Geol. Environ.* **2019**, *78*, 4167–4185. [CrossRef]
32. Wang, L.; Wang, L.; Wang, S.; Guo, F.; Zou, L. Numerical Analysis of Landslides Long-term Deformation Based on Creep Model of Unsaturated Soil. *J. Yangtze River Sci. Res. Inst.* **2019**, *36*, 113–120.
33. Yao, Z.; Chen, Z.; Fang, X.; Huang, X. Elastoplastic damage seepage-consolidation coupled model of unsaturated intact loess and its application. *Rock Soil Mech.* **2019**, *40*, 216–226.
34. Lei, X.; He, S.; Chen, X.; Wong, H.; Wu, L.; Liu, E. A generalized interpolation material point method for modelling coupled seepage-erosion-deformation process within unsaturated soils. *Adv. Water Resour.* **2020**, *141*, 103578. [CrossRef]
35. Zhang, W.; Shen, Z.; Ren, J.; Bian, J.; Xu, L.; Chen, G. Multifield Coupling Numerical Simulation of the Seepage and Stability of Embankment Dams on Deep Overburden Layers. *Arab. J. Sci. Eng.* **2022**, *47*, 7293–7308. [CrossRef]
36. Liu, Z.; Zhang, R.; Liu, Z.; Zheng, J. Influence of swelling anisotropy on stability of unsaturated expansive soil slope. *J. Cent. South Univ. Sci. Technol.* **2022**, *53*, 114–125.
37. Yeh, H.-F.; Tsai, Y.-J. Analyzing the Effect of Soil Hydraulic Conductivity Anisotropy on Slope Stability Using a Coupled Hydromechanical Framework. *Water* **2018**, *10*, 905. [CrossRef]
38. Formetta, G.; Capparelli, G. Quantifying the three-dimensional effects of anisotropic soil horizons on hillslope hydrology and stability. *J. Hydrol.* **2019**, *570*, 329–342. [CrossRef]
39. Xia, C.; Lu, G.; Zhu, Z.; Wu, L.; Zhang, L.; Luo, S.; Dong, J. Deformation and Stability Characteristics of Layered Rock Slope Affected by Rainfall Based on Anisotropy of Strength and Hydraulic Conductivity. *Water* **2020**, *12*, 3056. [CrossRef]
40. Yeh, P.-T.; Lee, K.Z.-Z.; Chang, K.-T. 3D Effects of permeability and strength anisotropy on the stability of weakly cemented rock slopes subjected to rainfall infiltration. *Eng. Geol.* **2020**, *266*, 105459. [CrossRef]
41. Wang, Z.; Wang, H.; Xu, W.; Xie, W.C. Slope stability analysis considering the rotated anisotropy in soil properties. *Eng. Comput.* **2021**, *38*, 3021–3035. [CrossRef]
42. Khan, K.U.J.; Wang, C.-m.; Khan, M.W.J.; Liang, Z.; Li, S.; Li, B.-l. Influence of rainfall infiltration on the stability of unsaturated coal gangue accumulated slope. *J. Mt. Sci.* **2021**, *18*, 1696–1709. [CrossRef]
43. Jing, X.; Chen, Y.; Pan, C.; Yin, T.; Wang, W.; Fan, X. Erosion Failure of a Soil Slope by Heavy Rain: Laboratory Investigation and Modified GA Model of Soil Slope Failure. *Int. J. Environ. Res. Public Health* **2019**, *16*, 1075. [CrossRef]
44. Wang, S.; He, J.; Yang, T. Numerical Analysis on Stability of Slope Considering Rainfall Infiltration. *J. Northeast. Univ. Nat. Sci.* **2018**, *39*, 1196–1200.
45. Zhang, Y.; Yuan, M.; Lu, W.; Zhang, J. Cause investigation of ground sliding during tunneling in sloping and stratified stratum. *Nat. Hazards* **2022**, *111*, 1421–1430. [CrossRef]
46. Liu, X.; Chen, X.; Su, M.; Zhang, S.; Lu, D. Stability Analysis of a Weathered-Basalt Soil Slope Using the Double Strength Reduction Method. *Adv. Civ. Eng.* **2021**, *2021*, 6640698. [CrossRef]
47. Wang, J.; Chapman, D.; Yang, X. Investigating the stability and anchor support parameters of slopes subjected to wetting and drying cycles in relation to the Nanfen open-pit mine, China. *Arab. J. Geosci.* **2020**, *13*, 1062. [CrossRef]